A new skill score for ensemble flood maps: assessing spatial spread-skill with remote sensing observations.

Helen Hooker[1], Sarah L. Dance[1,2,3], David C. Mason[4], John Bevington[5], and Kay Shelton[5]

[1]Department of Meteorology, University of Reading, UK
[2]Department of Mathematics and Statistics, University of Reading, UK
[3]National Centre for Earth Observation (NCEO), Reading, UK
[4]Department of Geography and Environmental Science, University of Reading, UK
[5]Jeremy Benn Associates Limited (JBA Consulting), UK

Correspondence: Helen Hooker (h.hooker@pgr.reading.ac.uk)

Abstract. An ensemble of forecast flood inundation maps has the potential to represent the uncertainty in the flood forecast and provide a location specific likelihood of flooding. Ensemble flood map forecasts provide probabilistic information to flood forecasters, flood risk managers and insurers and will ultimately benefit people living in flood prone areas. Spatial verification of the ensemble flood map forecast against remotely observed flooding is important to understand both the skill of the ensemble forecast and the uncertainty represented in the variation or spread of the individual ensemble member flood maps. In atmospheric sciences, a scale-selective approach has been used to evaluate a convective precipitation ensemble forecast. This determines a skilful scale (agreement scale) of ensemble performance by locally computing a skill metric across a range of length scales. By extending this approach through a new application we evaluate the spatial predictability and the spatial spread-skill of an ensemble flood forecast across a domain of interest. The spatial spread-skill method computes an agreement scale at every grid cell between each unique pair of ensemble flood maps (ensemble spatial spread) and between each ensemble flood map with a SAR-derived flood map (ensemble spatial skill). These two are compared to produce the final spatial spread-skill performance. These methods are applied to the August 2017 flood event on the Brahmaputra River in the Assam region of India. Both the spatial-skill and spread-skill relationship vary with location and are related to physical characteristics of the flooding event. Validation and mapping of the spatial spread-skill relationship in operational system monitoring would allow better quantification of forecast systematic biases and uncertainties. This would be particularly useful for ungauged catchments and would enable targeted model improvements to be made across different parts of the forecast chain.

1 Introduction

Forecast flood maps indicating the extent and depth of fluvial flood within an actionable lead time, are a useful tool for flood risk managers and emergency response teams prior to and during a flood event. Typically, forecast flood maps are presented as deterministic forecasts showing precisely where flooding will occur. This can lead to incidents of false alarms or missed warnings and subsequent recriminations causing mistrust in the system (Arnal et al., 2020; Savage et al., 2016). A timely prediction of exactly where and when fluvial flooding caused by intense or prolonged rainfall will occur is virtually impossible

due to the chaotic nature of the atmosphere (Lorenz, 1969). The ensemble forecasting approach aims to address the sensitive nature of the atmosphere to its initial conditions and through multiple model runs these initial condition uncertainties can be quantified (Leutbecher and Palmer, 2008). The ensemble forecast results in a probabilistic weather forecast that indicates the predictability of the atmosphere at a given space and time. State-of-the-art operational ensemble flood forecasting systems link together a chain of forecast models to produce probabilistic streamflow and flood inundation forecasts at national and global scales (Cloke and Pappenberger, 2009; Emerton et al., 2016; Wu et al., 2020). Ensemble Numerical Weather Prediction (NWP) models provide meteorological inputs into land-surface, hydrological and hydraulic models, cascading the atmospheric uncertainty through to the flood forecast. Throughout this chain of models multiple sources of uncertainties exist (Beven, 2016; Matthews et al., 2022; Pappenberger et al., 2005; Zappa et al., 2011). As discussed by Boelee et al. (2019), these uncertainties include those arising from meteorological inputs, measurements and observations, initial conditions, unresolved physics within the models and parameter estimates. A probabilistic flood inundation forecast should present a meaningful prediction of the likelihood of flooding so that there is confidence in the forecast, given the uncertainties represented in the system (Alfonso et al., 2016).

The accuracy of the location of flooding, predicted in advance, is defined as spatial predictability. The spatial predictability of ensemble forecasts of flood inundation could be verified by comparing with a remote observation of the flood from satellite or unmanned aerial vehicle (UAV) based sensors. Satellite-based optical and Synthetic Aperture Radar (SAR) sensors are well known for their flood detection capability (e.g. Horritt et al., 2001; Mason et al., 2012). SAR sensors are active, which enables them to scan the Earth through weather and clouds, and at night. The SAR backscatter intensity detected depends on the roughness of the surface, with unobstructed flooded areas and other surface water bodies appearing relatively smooth and returning low backscatter values. Dasgupta et al. (2018a) detail some of the challenges along with approaches to solutions of flood detection using SAR, examples of these challenges include: roughening of the water surface by heavy rain and strong wind, emergent or partially submerged vegetation and flood detection in urban areas. Accurate flood detection in urban areas particularly due to surface water flooding has become increasingly important (Speight and Krupska, 2021) and recent techniques have led to improved flood detection (Mason et al., 2018, 2021a, b). Optical instruments rely on solar energy and cannot penetrate cloud, making them less useful during a flooding situation. Recent studies have investigated the flood detection benefits from combining both optical and SAR imagery (Konapala et al., 2021; Tavus et al., 2020). Improvements in the spatial-temporal resolution of SAR images and their open source availability mean that they are an increasingly valuable tool for hydraulic and hydrodynamic model improvements through calibration, validation and data assimilation (e.g. García-Pintado et al., 2015; Hostache et al., 2018; Cooper et al., 2018, 2019; Di Mauro et al., 2021; Dasgupta et al., 2018b, 2021a, b). The Global Flood Monitoring (GFM) product (EU Science Hub, 2021; GFM, 2021; Hostache, R., 2021) of the Copernicus Emergency Management Service (CEMS) (Copernicus Programme, 2021) produces SAR-derived flood inundation maps for every Sentinel-1 image detecting flooding. Three flood detection algorithms provide uncertainty estimation and population affected estimates within 8 hours of the image acquisition. The European Space Agency (ESA) Copernicus Programme have recently included the ICEYE constellation of small satellites into the fleet of missions contributing to Europe's Copernicus environmental moni-

toring programme (ESA, 2021). ICEYE captures very high resolution (spot mode ground range resolution = 1 m) SAR images which brings the potential for increased accuracy of flood detection, particularly in urban areas.

60

To evaluate the accuracy of an ensemble forecast, a number of verification measures have been proposed. Anderson et al. (2019) developed a joint verification framework for end-to-end assessment of the England and Wales Flood Forecasting Centre (FFC) ensemble flood forecasting system. Anderson et al. (2019) describe verification metrics such as the continuous rank probability score (CRPS), rank histograms, Brier Skill Score (BSS) and the relative operative characteristics (ROC) diagrams

65   that are commonly applied to assess the main ensemble attributes desirable in both precipitation and streamflow ensemble forecasts (e.g. Renner et al., 2009). These metrics refer to flooding events as part of a time series evaluated against a reference benchmark, such as climatology, to produce an average skill score. In contrast, here we consider ensemble *spatial* verification at a single time point. The verification of ensemble forecasts usually involves comparing the RMSE of the ensemble mean against an observed quantity to assess the *skill* of the forecast with the ensemble standard deviation used as a measure of

70   *spread*. A perfect ensemble should encompass forecast uncertainties such that the ensemble spread is correlated to the RMSE of the forecast (Hopson, 2014). This *spread-skill* relationship was assessed by Buizza (1997) to investigate the predictability limits of the European Centre for Medium-Range Weather Forecasts (ECMWF) Ensemble Prediction System (EPS). This approach to ensemble verification is based on point values and makes the assumption that the ensemble mean is the forecast state with the highest probability and that the forecast distribution is Gaussian. Significant flooding events are, in their nature,

75   a rare occurrence and in certain circumstances a few ensemble members can indicate a low probability of an extreme flood. Also, in particular atmospheric scenarios the ensemble forecast may result in a multi-modal forecast where two clusters of ensemble members are each equally likely (Galmiche et al., 2021). For example, both clusters may indicate flooding events but at different magnitudes. In both of these instances the individual ensemble member details are important and evaluation of the ensemble mean alone would not be meaningful. When mapping the flood extent prediction, the ensemble mean field alone

80   does not retain the spatial detail of the individual member forecasts.

The spatial spread-skill of the ensemble forecast is determined by evaluating the full ensemble against observations of flooding. For a flood map ensemble to be considered spatially well-spread, the spread or variation between ensemble members should equal the spatial predictability, or skill of the ensemble members (Dey et al. (2014), see Section 2). Presently, to the best

85   of our knowledge, quantitative evaluation methods assessing the spatial spread-skill of ensemble forecast flood maps do not exist. However, previous work in numerical weather prediction by Ben Bouallègue and Theis (2014) investigated the application of spatial techniques to ensemble precipitation forecasts using a neighbourhood, or fuzzy approach that allowed comparisons at larger scales than grid level. A location dependent approach to the spatial spread-skill evaluation of a convective precipitation ensemble forecast was developed by Dey et al. (2016). This method compares every ensemble member across a range of scales

90   on a spatial field against an observation field to assess whether the ensemble forecast is spatially over-, under- or well-spread on average across a domain of interest (Chen et al., 2018). In a recent study, a scale-selective approach was developed and applied to evaluate a deterministic flood map forecast where comparisons were made against conventional binary performance

measures (Hooker et al., 2022a). The work described here extends and applies this scale-selective approach to assess the spatial predictability and the spatial spread-skill of an ensemble flood map forecast.

95

In this paper we aim to address the following questions:

- How can we summarise the spatial predictability information in ensemble flood map forecasts?

- How can we evaluate the spatial spread-skill of an ensemble flood map forecast?

- How does the spatial spread-skill vary with location and how can this be presented?

100 In Section 2 we present a new approach to the evaluation of spatial predictability and the spatial spread-skill of an ensemble flood map forecast by comparing against a remotely observed flooding extent. We illustrate the features of the methods through an example case study of an extreme flooding event of the Brahmaputra River which impacted India and Bangladesh in August 2017; with focus on the Assam region of India. The flood event details are described in Section 3.1. The international ensemble version of the JBA Consulting Flood Foresight system provides forecast flood maps for the study and is described in Section 105 3.2. Observations of the flood are derived from satellite based Synthetic Aperture Radar (SAR) sensors and the method is explained in Section 3.3. The results including our new Spatial spread-skill (SSS) map are discussed in Section 4. Our results show that individual ensemble member spatial predictions of flooding are meaningful and that the full ensemble spatial detail should be evaluated. We conclude in Section 5 that the spatial spread-skill of the ensemble forecast varies with location across the domain and can be linked to physical characteristics of the flooding event.

2 Ensemble flood map spatial predictability evaluation methods

110

In this Section we present new methods for evaluating and visualising the spatial-spread skill of an ensemble flood map forecast. Hooker et al. (2022a) described and applied a new scale-selective approach to evaluate the spatial skill of a *deterministic* flood map forecast relative to an observed SAR-derived flood map. Here, we apply this same measure to evaluate different aspects of an *ensemble* forecast. The scale-selective Fraction Skill Score (FSS) method is outlined in Section 2.1. Agreement scale 115 maps indicating forecast accuracy are defined for location-specific comparisons between forecast and observed flood maps in Section 2.2. These are used to assess the spatial relationship between each unique pair of ensemble member flood maps (member-member) and between every ensemble member flood map and the observed SAR-derived flood map (member-SAR, Section 2.3). Visualisation methods of the spatial spread-skill relationship including our new *Spatial Spread-Skill (SSS)* map are presented in Section 2.4.

2.1 Fraction Skill Score

120

The FSS is a scale-selective verification measure that can determine the skilful scale of a modelled flood map, when compared against a remotely sensed observation of flooding (Hooker et al., 2022a). We will call these flood maps the *model array* and

the *observed array* respectively. For an ensemble forecast, the model array could be an individual ensemble member, or a summarised flood estimate derived from a combination of ensemble members such as a combined ensemble or the ensemble median (see Section 3.4). Both the model and observed arrays are converted into binary fields using a situation dependent threshold. For this ensemble application of the FSS we evaluate the entire flood extent across the domain. Each grid cell is labelled as inundated (1) or dry (0). All grid cells are numbered according to their spatial locations (i, j), $i = 1 \ldots N_x$ and $j = 1 \ldots N_y$ where N_x is the number of columns and N_y is the number of rows. Surrounding each grid cell, a square of length n creates an $n \times n$ neighbourhood. The fraction of $1s$ (inundated cells) in the square neighbourhood area is calculated for every grid cell. This creates two arrays of fractions across the domain for both the observed O_{nij} and modelled M_{nij} data. The mean squared error (MSE) for the fraction arrays is calculated for the domain and a given neighborhood size, n:

$$MSE_n = \frac{1}{N_x N_y} \sum_{i=1}^{N_x} \sum_{j=1}^{N_y} [O_{nij} - M_{nij}]^2. \tag{1}$$

Depending on the fractions calculated for the model and observed fields a maximum MSE is calculated as:

$$MSE_{n(ref)} = \frac{1}{N_x N_y} \sum_{i=1}^{N_x} \sum_{j=1}^{N_y} [O_{nij}^2 + M_{nij}^2]. \tag{2}$$

Finally, the FSS is

$$FSS_n = 1 - \frac{MSE_n}{MSE_{n(ref)}}. \tag{3}$$

The FSS is initially calculated for the smallest neighbourhood size ($n = 3$) before increasingly larger neighbourhood sizes ($n = 5$, $n = 7$...) are considered. The FSS ranges between 0 (no skill) and 1 (perfect skill). Increasing the neighbourhood size typically leads to an improved FSS as the fractions are calculated over a larger area. Plotting FSS against the neighbourhood size can indicate a range of scales where the model is deemed to be the most skilful. A target FSS score (FSS_T) can be determined from the fraction of observed flooding across the whole domain (f_0)

$$FSS_T \geq 0.5 + \frac{f_o}{2}. \tag{4}$$

The point where the FSS_n exceeds FSS_T can be viewed as being equidistant between the skill of a random forecast and perfect skill (Roberts and Lean, 2008). The magnitude of the observed flood, relative to the domain area, determines the value of FSS_T. This allows the comparison of the skilful scale (neighbourhood size) where FSS_T is reached across different domain sizes and floods of different magnitudes.

2.2 Location dependent agreement scales

The FSS (Section 2.1) gives a domain average measure of forecast performance and a minimum spatial scale at which the forecast is deemed skilful. To enable the spatial spread-skill of the full ensemble to be evaluated at specific locations, we first

define an agreement scale (see Hooker et al. (2022a) for full methodology). The agreement scale is calculated and mapped for every grid cell in the domain and shows a measure of similarity between two arrays of data. In contrast to the FSS method the arrays are not required to be thresholded. The agreement scale method can be applied to both binary flood extent maps as well as flood depth fields. These could both be ensemble member flood maps or an ensemble member flood map and an observed flood map. Two data arrays are compared f_{1ij} and f_{2ij} and the aim is to find a minimum neighbourhood size (or spatial scale) for every grid cell such that there is a predetermined acceptable minimum level of agreement between f_{1ij} and f_{2ij}. This is known as the agreement scale $S_{ij}^{A(f_1 f_2)}$. (Note that the relationship between the agreement scale and the neighbourhood size described previously in section 2.1 is given by $S_{ij}^{A(f_1 f_2)} = (n-1)/2$.)

A relative MSE D_{ij}^S is calculated for all grid cells, initially at grid level, $S = 0$ ($n = 1$),

$$D_{ij}^S = \frac{(f_{1ij}^S - f_{2ij}^S)^2}{(f_{1ij}^S)^2 + (f_{2ij}^S)^2}. \tag{5}$$

If $f_{1ij} = 0$ and $f_{2ij} = 0$ (both dry) then $D_{ij}^S = 0$ (correct at grid level). The value of D_{ij}^S ranges between zero and 1. The arrays are deemed to be in agreement at the scale being tested if:

$$D_{ij}^S \leq D_{crit,ij}^{S_{ij}} \quad \text{where} \quad D_{crit,ij}^S = \alpha + (1-\alpha)\frac{S}{S_{lim}} \tag{6}$$

The parameter value α indicates an acceptable bias at grid level such that $0 \leq \alpha \leq 1$ and S_{lim} is a fixed maximum scale that is predetermined. We set the criterion for no background bias, $\alpha = 0$. If $D_{ij}^S \geq D_{crit,ij}^S$ then the next neighbourhood size up is considered ($S = 1$, $n = 3$, a 3 by 3 square) where f_{1ij}^1 and f_{2ij}^1 are the average value of each neighbourhood surrounding the grid cell at position (i,j) for each array. The process continues by comparing increasingly larger neighbourhoods (e.g. $S = 2$, $n = 5$, a 5 by 5 square) until the agreement criterion

$$S_{ij}^{A(f_1 f_2)} \quad \text{or} \quad S_{lim} \quad \text{at} \quad D_{ij}^S \leq D_{crit,ij}^{S_{ij}} \tag{7}$$

is met for every cell in the domain. The agreement scale at which the agreement criterion is met will usually vary from grid cell to grid cell and these values ($S = 0$, $S = 1$, $S = 2$ and so on up to S_{lim}), each specific to each grid cell location can be mapped onto the domain of interest to provide a location specific measure of agreement between the two data arrays that are compared.

A categorical scale map shows a measure of spatial accuracy between two data arrays (Hooker et al., 2022a). Validation of forecast flood maps against remotely observed flooding extent is typically carried out by labelling each grid cell using a contingency table with categories: correctly predicted flooded, under-prediction (miss), over-prediction (false alarm) and correctly predicted unflooded. Mapping these categories creates a conventional contingency map, which combined with an agreement scale map creates a categorical scale map. Categorical scale maps may be used as a basis for comparison between ensemble members and observations, as we illustrate with our case study in Section 4.3.

2.3 Ensemble spatial spread-skill evaluation

We assume that each ensemble forecast flood map represents an equally likely future scenario and the evaluation of the full ensemble is needed to quantify the uncertainty and to evaluate the spatial spread-skill relationship. The ensemble flood map spatial characteristics vary with location and in order to preserve the location dependent information, we utilise a method developed to evaluate a convective ensemble precipitation forecast (Dey et al., 2016). Here, we outline the method and describe a new application to evaluate an ensemble forecast flood map.

A neighbourhood approach (Section 2.2) is used to assess the spatial agreement scale $S_{ij}^{A(f_1 f_2)}$ or measure of similarity at each grid cell location (i, j) between each unique pair of ensemble flood maps. For an ensemble of M members, there are

$$M_p = \frac{M(M-1)}{2}, \tag{8}$$

unique pairs (e.g., 1275 pairs for a 51 member ensemble). For an ensemble, the skillful scale can be renamed as a *believable scale*, which is the scale where ensemble members become sufficiently similar to observations such that they are a useful prediction. Every paired ensemble agreement scale field is averaged at each grid cell to produce a mean field, following from equation (7)

$$S_{ij}^{A(\overline{mm})} = \frac{1}{M_p} \sum_{f_1=1}^{M-1} \sum_{f_2=f_1+1}^{M} S_{ij}^{A(f_1 f_2)} \tag{9}$$

indicating the location specific believable scales of the forecast flood map ensemble. Maps of $S_{ij}^{A(\overline{mm})}$ summarise the spatial spread of the full ensemble. Each of the agreement scale fields between the ensemble members and the observations are also averaged at each grid cell to give

$$S_{ij}^{A(\overline{mo})} = \frac{1}{M} \sum_{f=1}^{M} S_{ij}^{A(f_0)}. \tag{10}$$

A measure of the spatial spread-skill of the ensemble can be found by comparing the average agreement scale between the ensemble members $S_{ij}^{A(\overline{mm})}$ representing the ensemble *spread* with the average agreement scale between the ensemble members and the observed flood field $S_{ij}^{A(\overline{mo})}$ representing the ensemble *skill*.

2.4 Spatial spread-skill visualisation methods

To evaluate the spatial spread-skill relationship, $S_{ij}^{A(\overline{mm})}$ (representing the ensemble *spread*) must be compared in the same location as $S_{ij}^{A(\overline{mo})}$ (representing the ensemble *skill*). Data arrays can be visually compared using a binned scatter plot that averages across a selected bin of cells at the same location within the domain. Dey et al. (2016) demonstrated for an idealised example that by plotting $S_{ij}^{A(\overline{mm})}$ against $S_{ij}^{A(\overline{mo})}$ as a binned scatter plot in order to preserve the spatial location of the comparison (Fig. 1), the ensemble can be classified as over-, under- or well-spread. The ensemble is deemed to be *well-spread* at a specific location in the domain of interest when the spread of the individual members represented at each grid cell by $S_{ij}^{A(\overline{mm})}$

equals the skill of the ensemble represented at each grid cell by $S_{ij}^{A(\overline{mo})}$, i.e. $S_{ij}^{A(\overline{mm})} - S_{ij}^{A(\overline{mo})} = 0$. The result would lie on a 1:1 line on the binned scatter plot. Where the spread between the ensemble members exceeds the skill of the ensemble forecast i.e. $S_{ij}^{A(\overline{mm})} > S_{ij}^{A(\overline{mo})}$ the ensemble is considered to be *over-spread* and the binned scatter plot will lie beneath the 1:1 line. The converse is true for an *under-spread* ensemble forecast where the agreement between members, the spread, is less than the

215 agreement between the ensemble and the observations, the skill. Here, $S_{ij}^{A(\overline{mm})} < S_{ij}^{A(\overline{mo})}$ and the binned scatter plot would lie above the 1:1 line.

To summarise the spread-skill relationship we develop this visualisation further by plotting a hexagonal binned 2D histogram plot (an example hexbin plot is presented in Section 4.3). The domain is divided into a (pre-determined) number of hexagons.

220 Hexagons minimize the perimeter to area ratio and therefore minimize the edge effects. The hexbin histogram plot colour shade represents the number of data points within each bin.
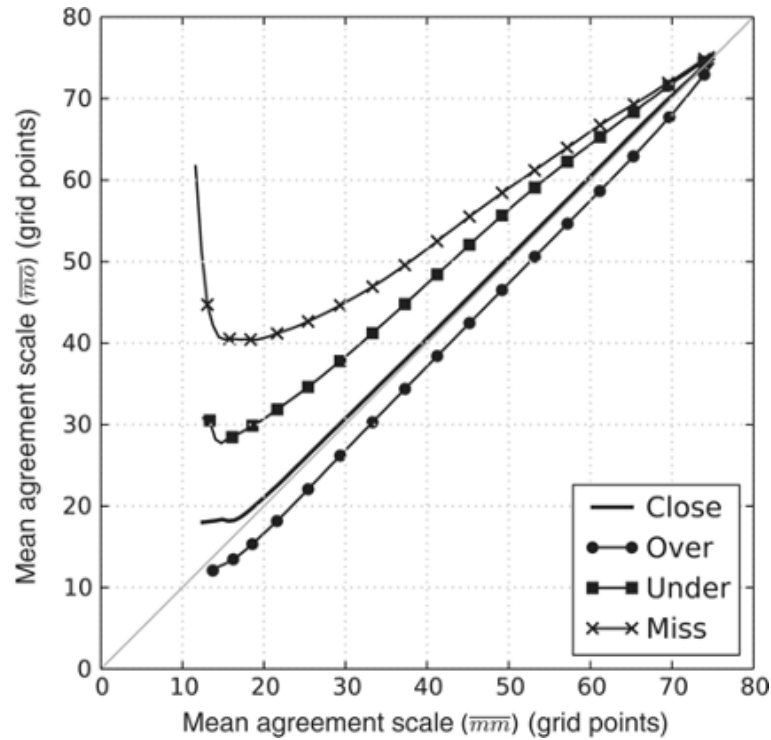
Figure 1. Figure reproduced with permission from Dey et al. (2016) showing results from an idealised experiment indicating the spatial spread-skill relationship between an ensemble forecast and the observation.

Whilst the hexbin plot is useful for gaining an understanding of the general spread-skill relationship of the ensemble flood map forecast, it does not tell us specifically where in the domain the ensemble spatial predictability is better or worse so that it

225 can be linked to physical processes and to improve aspects of the flood forecasting modelling chain. Our new *Spatial Spread-*

Skill (SSS) map plots $S_{ij}^{A(\overline{mm})} - S_{ij}^{A(\overline{mo})}$ at every grid cell location so that the spread-skill is mapped across the domain and can be linked directly to different sub-catchments and surface features such as tributaries, embankments, bridges and importantly the underlying topography or DTM, which influence the derivation of the ensemble flood maps. Regions on the SSS map where the ensemble is over-spread are positive with negative areas indicating where the ensemble is under-spread, zero values show a well-spread ensemble. Note that this does not necessarily mean that the entire ensemble is in agreement with observations at grid level, but that the agreement scales between $S_{ij}^{A(\overline{mm})}$ and $S_{ij}^{A(\overline{mo})}$ are equal. (An example SSS map is presented in Section 4.3).

3 Ensemble forecasting flood event case study

In this section we describe an example flooding event used to demonstrate the application of our new spatial spread-skill evaluation approach. We evaluate a 1-day flood inundation 51 ensemble member forecast from the Flood Foresight system (Section 3.2) for the domain area against a satellite SAR-derived flood map (Section 3.3).

3.1 Brahmaputra flood, Assam India, August 2017

The origin of the Brahmaputra River (also known as the Yarlung Tsangpo in Tibetan, the Siang/Dihang River in Arunachali, Luit in Assamese, and the Jamuna River in Bangladesh) lies in the Himalayan Kailas Range of southwestern Tibet, China. Draining an area of 543,000 km^2, the Brahmaputra flows for 2000 km across the Tibetan Plateau and a further 1000 km parallel to the Himalayan foothills through the Assam Valley, India before entering Bangladesh where the Brahmaputra joins the Ganges River (Palash et al., 2020). The Brahmaputra baseflow originates from the upstream glacial snow melt, however the streamflow rates are dominated by the summer monsoon precipitation. The basin receives up to 95% of its annual rainfall during the pre-monsoon and monsoon season, which usually runs from April to September and causes annual flooding of the Brahmaputra. The Assam region typically records on average 2300 mm of annual rainfall and up to 5000 mm in the Himalayan foothills (Dhar and Nandargi, 2000, 2003).

For this example case we focus on the third wave of flooding that occurred during the monsoon season in August 2017, peaking around the 12th. Figure 2 shows the location of the Brahmaputra and of a chosen domain centred upon some of the worst flooding that occurred. This area includes a confluence zone where the Subansiri River meets the Brahmaputra. The monsoon flooding impacted an estimated 40 million people across India and Bangladesh. Locally in the Assam region, the flooding in August affected over 3.3 million people and approximately 3200 villages, river embankments were damaged in 11 districts. Over 14,000 people were evacuated to one of around 700 relief camps that were also needed to house over 180,000 people relocated (Floodlist, 2017). The local Assam State Disaster Management Authority (ASDMA, 2017) flood early warning system issued a low warning alert (disasters that can be managed at the district level) on the 10th August for the district.
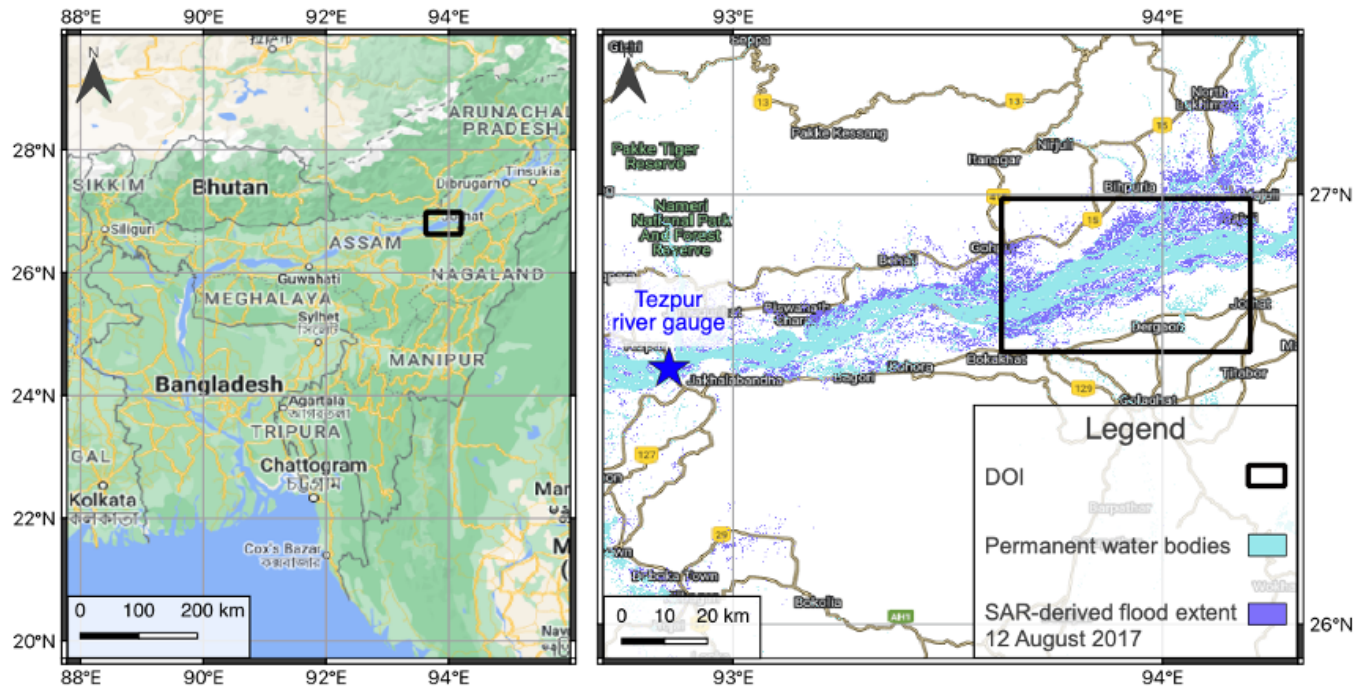
Figure 2. Left panel: domain location on the Brahmaputra River in the Assam region of India. Domain size is 57.5 km by 39.3 km. Right panel: Sentinel-1 SAR-derived flood map for the domain of interest. Base map from ©Google Maps.

In 2017, the southwest monsoon season rainfalls were predicted to be *normal* by the South Asian Climate Outlook Forum (WMO, 2017). However, the pre-monsoon season began early in the year with heavy thunderstorms affecting the region from March onwards. In the Assam region, June and July were 60% wetter than the previous three years and during August more locally intense rainfall was recorded compared with historical observations (Palash et al., 2020). In higher latitude areas, 30 km to the north of the domain at North Lakhimpur, 215.8 mm rainfall was recorded in the three days prior to the flood peak (Floodlist, 2017; Hossain et al., 2021). An above normal flood situation is declared in India where the river water level exceeds the Warning Level, a severe flood occurs where the water level exceeds the Danger Level, and an extreme flood occurs where the previous Highest Flood Level is exceeded (Central Water Commission, 2023). The peak water level recorded downstream at Tezpur (Danger Level 65.23 m) on August 14th was 66.12 m. There are regional variations in maximum water levels reported, with upland regions to the north of the Assam valley recording water levels that exceed the previous Highest Flood Level indicating an extreme flood level (Floodlist, 2017).

3.2 Ensemble flood forecasting system

The Flood Foresight system (Fig. 3), developed and operationally run by JBA Consulting, is a fluvial flood inundation mapping system that can be implemented at any river basin around the world. Flood Foresight utilises a simulation library approach to generate real-time and forecast flood inundation and water depth maps. The simulation library approach saves valuable computing time and allows the application of Flood Foresight in near continuous real-time at national and international scales. A pre-computed library of flood maps for a river basin or country are created using JFlow®, (Bradbrook, 2006) and RFlow. JFlow uses a raster-based approach with a detailed underlying digital terrain model (DTM) and a diffusion wave approximation of the full 2D hydrodynamic shallow water flow equations. RFlow combines a 1D model based upon Normal Depth calculations, optimised for use on a Digital surface Model (DSM, NEXTmap (2016)) with rapid 2D flood spreading (created by spreading Normal Depth from upstream to downstream) and is calibrated against JFlow. These equations capture the main controls of the flood routing for shallow, topographically driven flow. Six flood maps at 30 m resolution are created for 20, 50, 100, 200, 500 and 1500 year return period flood events (corresponding to annual exceedance probabilities (AEPs) of 5%, 2.5%, 1%, 0.5% and 0.2% and 0.07% respectively). Between each adjacent pair of modelled return period maps, five additional intermediate flood maps are created by linear interpolation. An additional five flood maps are also created beneath the lowest return period flood map. This gives, in total, a library of 36 flood maps. Note that these flood maps are undefended. Flood Foresight takes inputs of rainfall from numerical weather prediction (NWP) models, river gauge data (both historical and real-time) and forecast streamflow and uses these to select the most appropriate flood map for the location and forecasts daily flood maps out to ten days.

The global (non UK and Ireland) configuration of Flood Foresight uses ensemble streamflow forecast data from the Global Flood Awareness System (GloFAS) (Alfieri et al., 2013; GloFAS, 2021). GloFAS was jointly developed by the European Commission and the European Centre for Medium-Range Weather Forecasts (ECMWF) and is composed of an integrated hydro-meteorological forecasting chain that couples state-of-the-art weather forecasts with a land surface and hydrological model. With its continental scale set-up, GloFAS provides downstream countries with forecasts of upstream river conditions up to one month ahead as well as continental and global overviews for large world river basins. Meteorological forecast data are provided by the ECMWF Ensemble (IFS) model, the operational ensemble weather forecasting product of the ECMWF. The meteorological forecast data provide inputs to the land surface module, HTESSEL (Hydrological Tiled ECMWF Scheme for Surface Exchange over Land). HTESSEL simulates the land surface response to the meteorological data, based on simulated interactions with soil conditions, idealised vegetation cover and land cover. From these simulations, HTESSEL outputs forecast global surface and sub-surface flows per grid cell. These simulated flows are then used by a simplified version of the hydrological model LISFLOOD, a 1D routing model which simulates the movement of the surface and sub-surface flows. The runoff data produced is routed through a representation of the river network using a double kinematic wave approach, which includes bankfull and over bankfull routing. The river network used is taken from the HydroSHEDS dataset (Lehner and Grill,
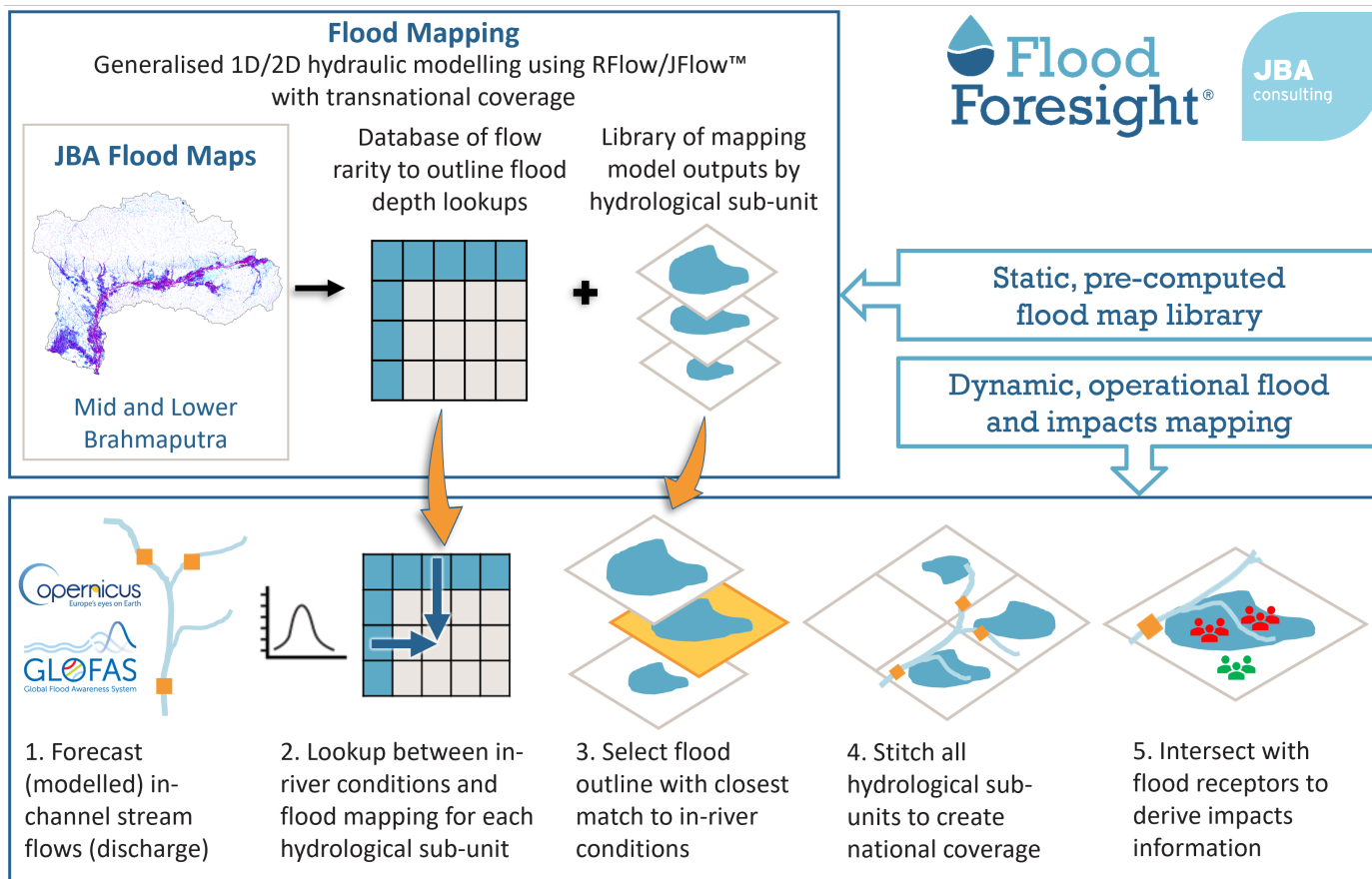
Figure 3. Flood Foresight ensemble forecast flood inundation and impact mapping work flow.

2013).

GloFAS outputs a gridded (approximately 10 km spatial resolution) ensemble forecast of river streamflow. Each of the GloFAS grid cells are linked to sub-catchments in the Flood Foresight system. The simulation library flood maps are selected when the forecast streamflow exceeds a return period threshold level. Each ensemble member flood map forecast is created by aggregating the individual sub-catchment maps. In summary, the meteorological IFS 51 member ensemble input to the flood forecasting chain allows atmospheric evolution uncertainties to be represented within the ensemble streamflow forecast and the ensemble of inundation flood maps, thus creating a probabilistic flood map forecast, indicating the likelihood of flooding.

3.3 SAR-derived flood map

A Sentinel-1 (S1A) image was acquired in interferometric wide swath mode (swath width 250 km) around the time of the flood peak at 17:18 (IST) on the 12th August 2017. The ESA Grid Processing on Demand (GPOD) HASARD service (http:

//gpod.eo.esa.int/) was utilised to map the flooding. The flood mapping algorithm (Chini et al., 2017) uses an automated, statistical, hierarchical split-based approach to distinguish between two classes (background and flood) using a pre-flood and flood image. A pre-flood image (February 2017) from the same satellite sensor and track was used to derive the flood map (Fig. 2). Original SAR images (VV) were pre-proccesed, which involved: precise orbit correction, radiometric calibration, thermal noise removal, terrain correction, speckle reduction and re-projection to the WGS84 coordinate system. The HASARD mapping algorithm removes permanent water bodies that are detected on the pre-flood image, such as the unflooded river water, lakes and reservoirs by applying a thresholding approach. Flooded areas beneath vegetation, bridges and near to buildings will not be detected using this method. Flood Foresight forecast flood maps include the river channel and exclude surface features such as vegetation and buildings. To smooth the HASARD flood maps and allow a fairer comparison we apply a morphological closing operation (without impacting the location of the flood extent) to flood fill vegetation and buildings. The wide and braided Brahmaputra River in the Assam region covers a significant area of the selected domain. So that the flood prediction accuracy alone can be evaluated, the pre-flood occurrence of surface water using the JRC Global Surface Water database (Pekel et al., 2016) has been removed from the Flood Foresight forecast inundation maps. The observed flood extent derived from satellite based SAR data at 20 m grid size is re-scaled to match the forecast flood map grid size (30 m) using average aggregation. The closest available (cloud free) optical image available was a Sentinel-2 image on the 17th August 2017, 5 days after the SAR image acquisition. During this time the flood waters had receded from their peak, which makes this unsuitable for comparison with the SAR-derived flood map. Since no other validation sources are available, for the purposes of this study we assume that the SAR-derived observation of flooding represents the true flooding extent. From October 2021, Sentinel-1 SAR images are processed by CEMS GFM (GFM, 2021) to derive flooding extent and provide an uncertainty estimate of the grid cell classification. This means uncertainty information in the SAR-derived flood map could be accounted for in future evaluation studies.

3.4 Forecast data

Flood Foresight was set-up for the Brahmaputra basin in India and Bangladesh using the simulation library approach to flood mapping described in Section 3.2. The forecast data for the Brahmaputra flood event contains a 51 member ensemble of flood maps indicating flooding extent, produced at a 1-day lead time. Vertically stacking each individual ensemble member flood map and adding vertically across every grid cell combines all ensemble members into a single flood map (all flooded grid cells are set to 1) showing where flooding is possible across all members (ens_{all}). A spatial median flood map is created (ens_{median}) where 26 members or more predict flooding at a particular grid cell location. Each of the ensemble member flood maps for the domain (Fig. 2) are plotted in Figure 4 along with ens_{all}, ens_{median} and the SAR-derived flood map.
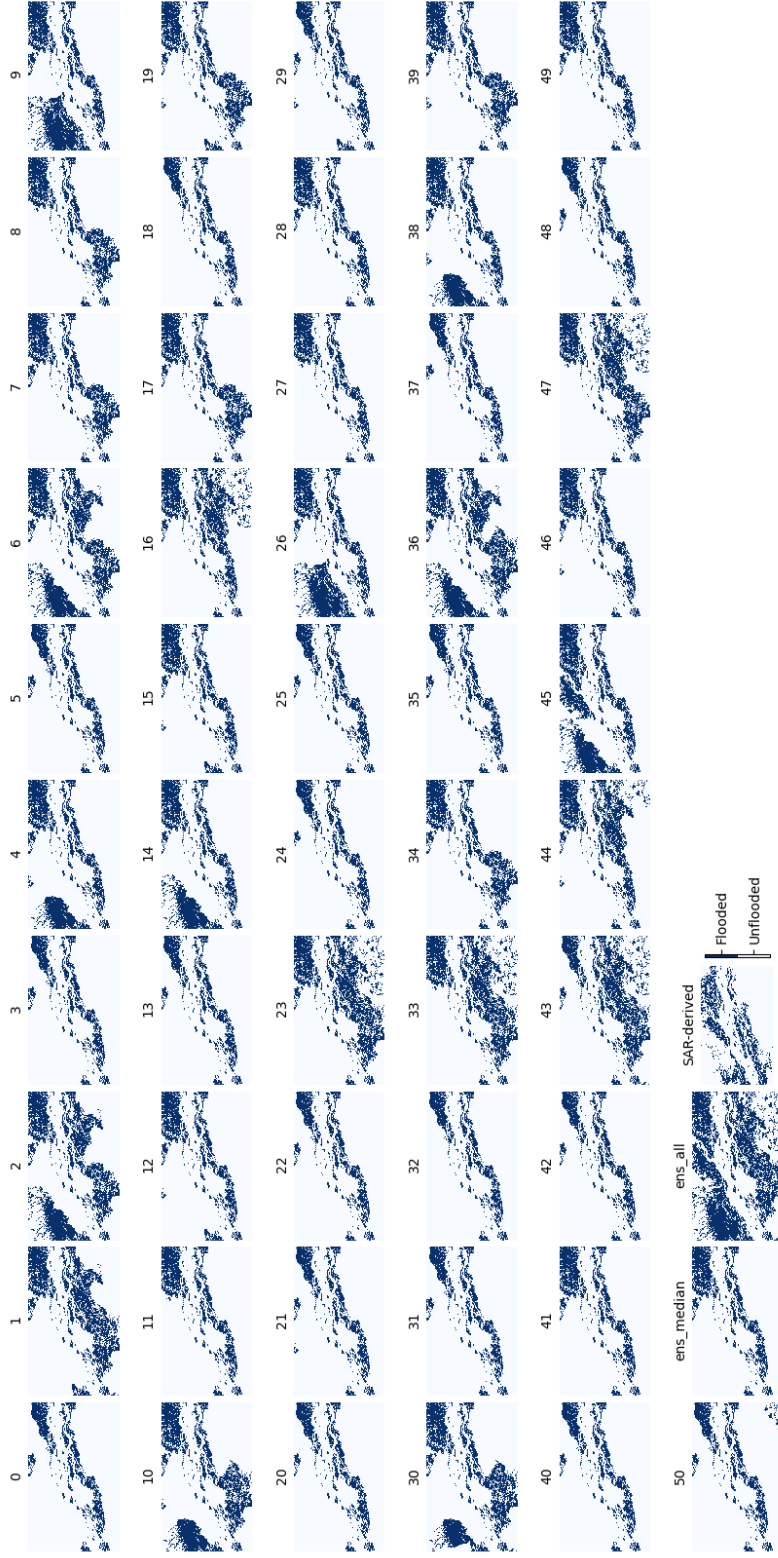
Figure 4. Brahmaputra River, Assam region, August 2017. 51 ensemble member forecast flood maps (labelled 0 to 50), ens_{median} and ens_{all} all at 1-day lead time and the Sentinel-1 SAR-derived flood map.

Figure 5 shows the amalgamated probabilistic ensemble forecast indicating the probability of flooding at each grid cell location. This was produced by vertically stacking each ensemble member flood map and adding vertically the number of flooded cells at each grid cell location across all ensemble members. The total is divided by 51 to calculate the probability. Dark blue colours near to the central river channel indicate agreement between all ensemble members and 100% forecast probability of flooding, lighter colours to the north of the river indicate a low probability of flooding.
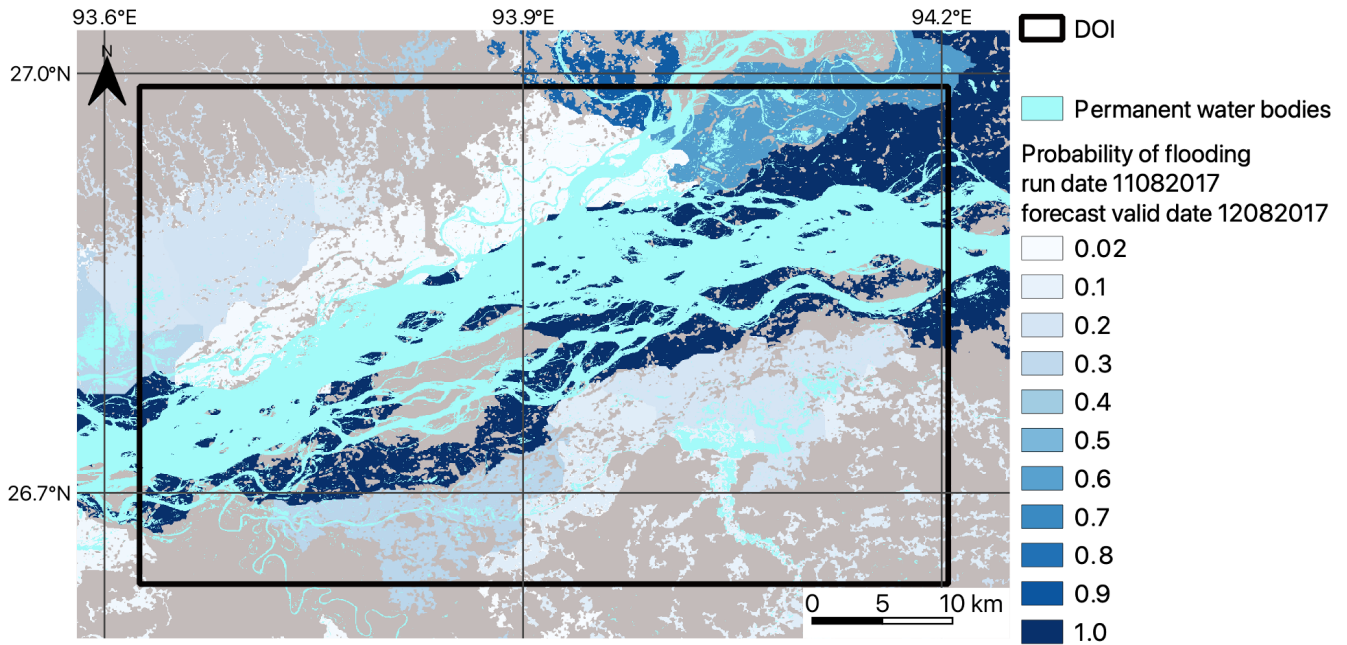
Figure 5. Brahmaputra River, Assam region, August 2017. Colour shading from white (low) to dark blue (high) indicate the forecast probability of flooding based on a 1-day lead time, 51 ensemble member flood map forecast for the Brahmaputra River in the Assam region, August 2017. (Note map background is grey)

4 Results and discussion

To demonstrate an application of our new spatial scale approach to both ensemble forecast flood map evaluation of forecast skill and the spatial spread-skill relationship, we apply the methods outlined in Section 2 to the flooding case described in Section 3.1. First, in Section 4.1 we verify the full ensemble using a spatial scale approach to calculate a skilful scale of agreement between each ensemble member and the SAR-derived flood map (Fig. 2) along with the combined ensemble (ens_{all}) and the ensemble spatial median (ens_{median}). We evaluate the location specific spatial skill of the ensemble by calculating categorical scale maps (Section 4.2) for ens_{all}, ens_{median} and a best and worst case ensemble members determined by the skilful scale

calculated in Section 4.1. In Section 4.3 we evaluate the spatial predictability of the full ensemble and show this on our new
Spatial Spread-Skill (SSS) map, indicating regions where the ensemble is over-, under- or well-spread.

4.1 Ensemble spatial scale evaluation

Here we investigate how a scale-selective approach can be useful for extracting meaningful information from a flood map
ensemble forecast where multiple forecast flood maps represent equally likely flooding scenarios (Fig. 4). A minimum skilful
scale (where $FSS > FSS_T$) has been calculated for each individual member flood map, ens_{all} and ens_{median}. The results in
Figure 6 show that individual ensemble member spatial skill varies considerably with FSS at grid level ranging from 0.35 to
0.59. One member ens_1, which would usually be disregarded as an outlier due to its low probability, outperformed all other
members significantly with a skilful scale achieved at a neighbourhood size of $n = 3$. The combined ens_{all} showed more skill
at grid level ($n = 1$) and smaller neighbourhood sizes compared with ens_{median}, both however exceeded FSS_T at $n = 41$, or
600 m. At neighbourhood sizes greater than $n = 41$, ens_{median} outperformed ens_{all}. There is a cluster of members showing
similar skill to ens_{median} and ens_{all} and a second cluster, with more ensemble variation but indicating lower skill than the
first cluster. The ens_{median} and ens_{all} flood maps outperform the second cluster, however there are individual members with
a higher spatial skill score compared to ens_{median} and ens_{all}. These results show that all ensemble member flood maps,
including outliers, should be considered individually as possible future flooding scenarios. Spatial variations across individual
ensemble members (see Fig. 4 ens_1 compared to ens_{median}) indicate that it is not meaningful to consider only the ensemble
median flood map to represent the information within the full ensemble.

4.2 Ensemble spatial predictability

The scale-selective skill scores calculated for different aspects of the ensemble forecast give a domain-averaged score and
skilful scale. To understand location specific spatial predictability of the ensemble forecast, categorical scale maps are cal-
culated and presented in Figure 7. These show how the agreement scale (Section 2.2) varies with location for (a) ens_{all}, (b)
ens_{median}, (c) ens_1, the 'best' performing ensemble member and (d) ens_{21}, the 'worst' performing ensemble member. The
ensemble summary map, ens_{all} (Fig. 7 (a)) captures most of the observed flooding (in grey) with small regions of under-
prediction (red). However, as you might expect to see by including every potential flooding realisation there are significant
regions of over-prediction (blue) or false alarm. The region of over-prediction to the south of the river is less evident in the
ens_{median} categorical scale map (Fig. 7 (b)) which performs worse to the north by under-predicting flooding here. This flood-
ing is captured well by ens_1 (Fig. 7 (c)) and in particular close to a confluence zone where the Subansiri River joins the
Brahmaputra (grid cell location (1100, 250)). This ties in with the high rainfall totals accumulated just to the north of this
region associated with localised very heavy rainfall (Floodlist, 2017). A region of under-prediction at grid cell location (750,
750) is missed by all members. A closer inspection of the DTM or surface features included/excluded in the hydraulic mod-
elling, such as embankment heights, may indicate how this modelling could be improved. The 'worst' performing ensemble
member ens_{21} (Fig. 7 (d)) accurately predicts flooding closer to the river channel, however under-prediction to the north along
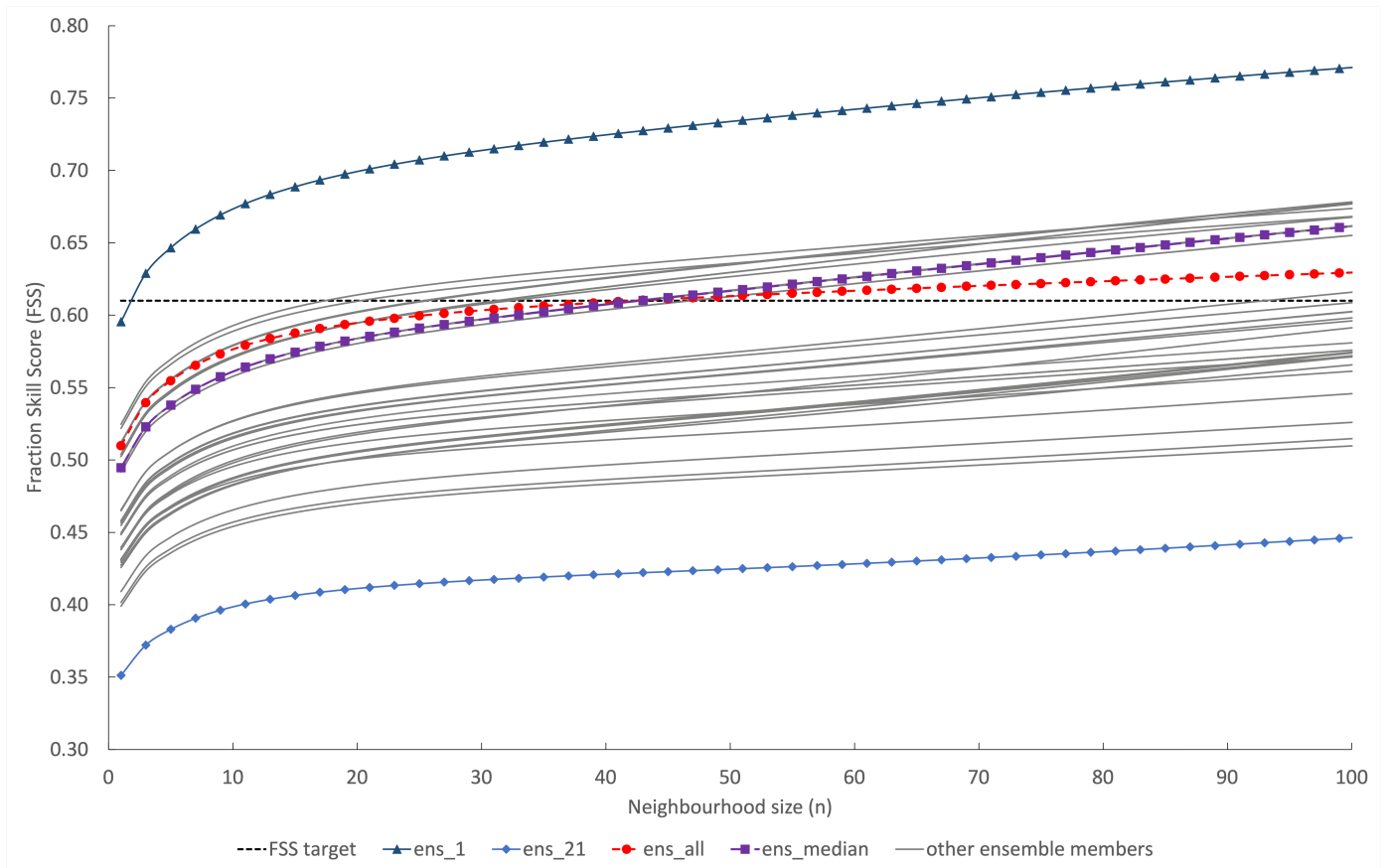
Figure 6. The spatial skill of each individual ensemble member forecast flood extent is evaluated along with the ens_{median} (a spatial median where 26 or more members predict flooding at a grid cell location) and ens_{all} (flooded grid cells from all ensemble members are combined). The FSS is calculated at increasing neighbourhood sizes to determine the scale at which the forecast becomes skilful at capturing the observed flood (FSS_T).

with over-prediction to the south show where the forecast was inaccurate. Categorical scale maps enable different ensemble flood map presentations to be evaluated so that the most useful presentation method can be determined for a particular flooding situation.

4.3 Ensemble spatial spread-skill

To evaluate the location specific skill of the full ensemble, one option would be to calculate 51 categorical scale maps from each individual member flood map (Fig. 4). This approach maintains the spatial detail held within each of the ensemble member flood maps, although does require multiple visual comparisons to be made by the flood forecaster or modeller, which takes time and effort. Making comparisons across the different ensemble member flood maps in Figure 4 provides a demonstration
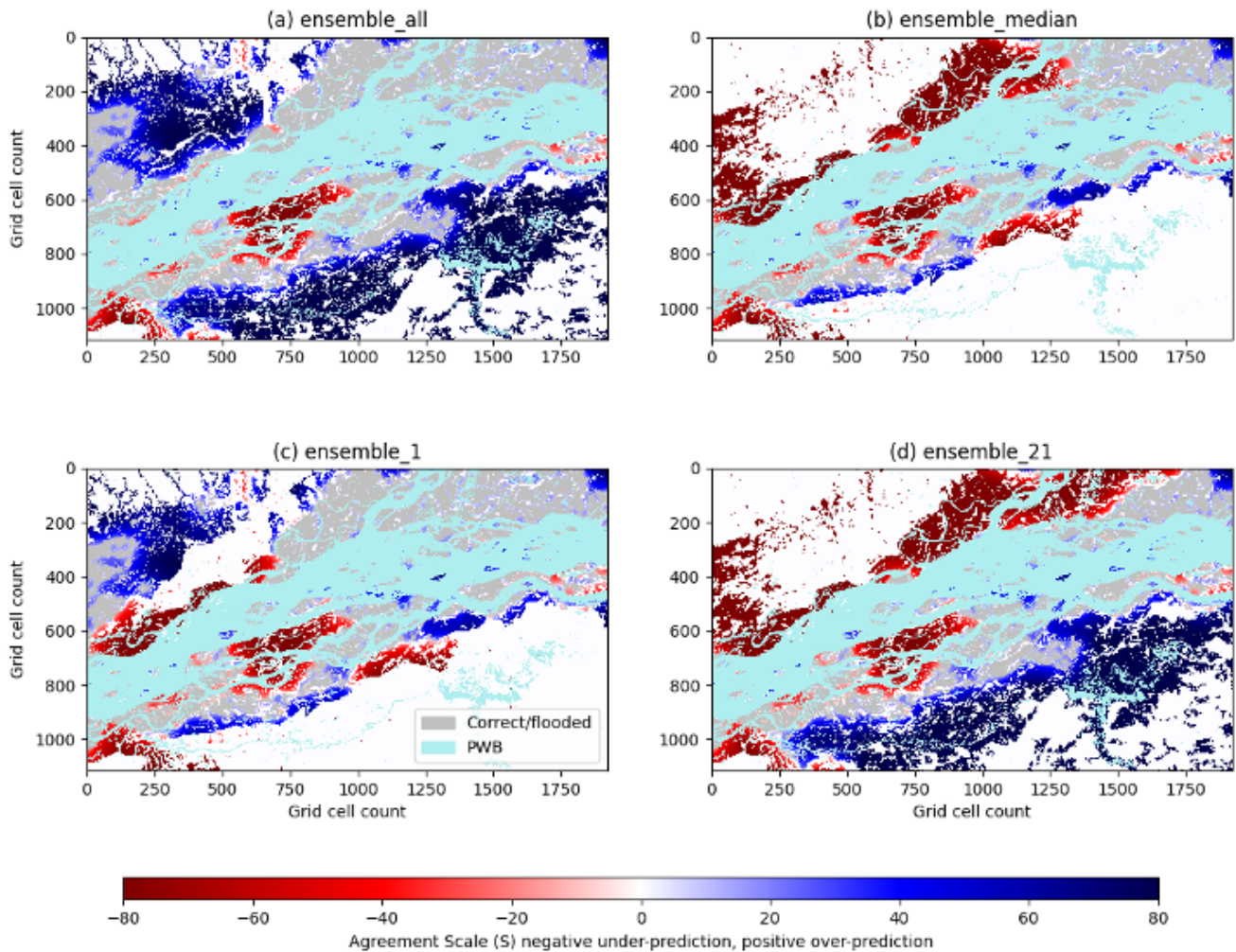
Figure 7. Brahmaputra River, Assam region, August 2017. Categorical scale maps for (a) ens_{all} (flooded grid cells from all ensemble members are combined), (b) ens_{median} (a spatial median where 26 or more members predict flooding at a grid cell location), (c) individual ensemble member 1 and (d) individual ensemble member 21. Red areas indicate where the forecast is under-predicted and blue regions represent over-prediction. The colour shade gives the scale of agreement between the forecast and the observed flooding with lighter shading indicating a smaller agreement scale. For georeferencing see Figure 5, each grid cell is 30 m x 30 m.

395   of these forecasting difficulties. Further, the categorical scale maps do not evaluate the ensemble spatial spread. To address this, we develop a Spatial Spread-Skill (SSS) map (Fig. 9) showing the spread-skill of the full ensemble forecast and keeping the location specific detail. All ensemble members are included in this analysis which evaluates both the spatial skill and the ensemble spatial spread of the forecast against the remotely observed flooding extent.

Figure 8 shows how the average-ensemble/ensemble-agreement scale in (a) $S_{ij}^{A(\overline{mm})}$ calculated at each grid cell (representing ensemble *spread*) compares with the average ensemble/observed scale in (b) $S_{ij}^{A(\overline{mo})}$ (representing ensemble *skill*) along with the hexbin scatter plot in (c) which compares (a) and (b) to indicate the spatial spread-skill of the forecast. The hexagonal tessellation is used so that the distances along the hexbin diagonal are on the same scale as those along the x and y-axis. For a perfect ensemble forecast the average agreement scale between ensemble members should match the agreement scale between the ensemble forecast and observed flood map, i.e. they should align along the 1:1 line. The SSS map plots the difference between the ensemble/ensemble and the ensemble/observed average agreement scales at each grid cell (Fig. 9) and indicates where the spatial spread-skill is over-, under-, or well-spread. Three numbered areas (Fig 8(a)) identify three different ensemble spread-skill relationships. Area 1 shows that the agreement between ensemble members is close, but that they disagree with the observed flooding extent. This is displayed in orange shades as an under-spread or miss region on the SSS map, Figure 9. This is the region close to the confluence area described in Section 4.2. Recall that in this region, most ensemble members did not predict the flooding that occurred with the exception of one ensemble member (ens_1). In area 2 on Figure 8, both (a) and (b) are in agreement at grid level, which indicates the ensemble is well-spread; these are shown in white on Figure 9. Away from the miss and well-spread regions in Figure 8, the overall visual impression is that the ensemble spread-skill lies below the 1:1 line and is over-spread, indicated by area 3. This corresponds to purple shading on the SSS map (Fig. 9). Overall Figure 8 tells us that the spread-skill relationship for this example case study is not uniform across the domain but is in fact location specific. Using the spatial spread-skill relationship shown on the ensemble SSS map we can infer how well the ensemble forecasting system encompasses the multiple sources of uncertainty and how meaningful the probabilistic ensemble forecast of flood inundation actually is. This is a useful evaluation tool for validating flood forecasts in un-gauged or partially gauged rivers. A simulation library approach, like the Flood Foresight maps used here, relies on the accuracy of the return period thresholds set, the (ensemble) forecast streamflow and the accuracy of the flood inundation map for a given streamflow. The forecast evaluation approaches presented here enable these system attributes to be evaluated even where observed streamflow is limited or erroneous. The SSS map summarises the whole ensemble, which makes it useful for forecasters attempting to convey uncertainty information to decision makers, highlighting regions where there is high/low confidence in the forecast.
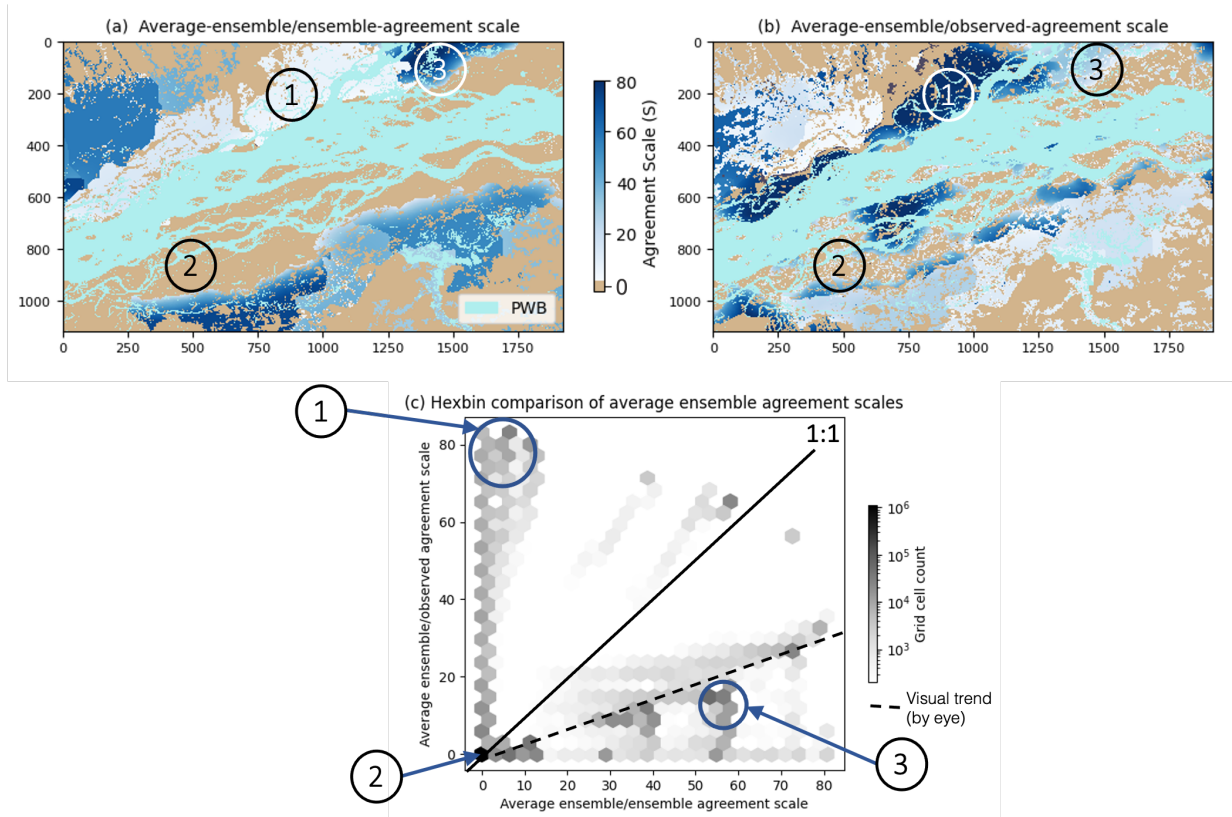
Figure 8. Brahmaputra River, Assam region, August 2017. (a) The average agreement scale map of each unique pair of forecast ensemble flood maps and (b) between each ensemble member compared against the observed SAR-derived flood map. (c) A binned histogram scatter plot compares (a) and (b) to indicate the spatial spread-skill of the forecast ensemble. Areas labelled (1, 2 and 3) are discussed in Section 4.3. For georeferencing of (a) and (b) see Figure 5. Note PWB means permanent water bodies.
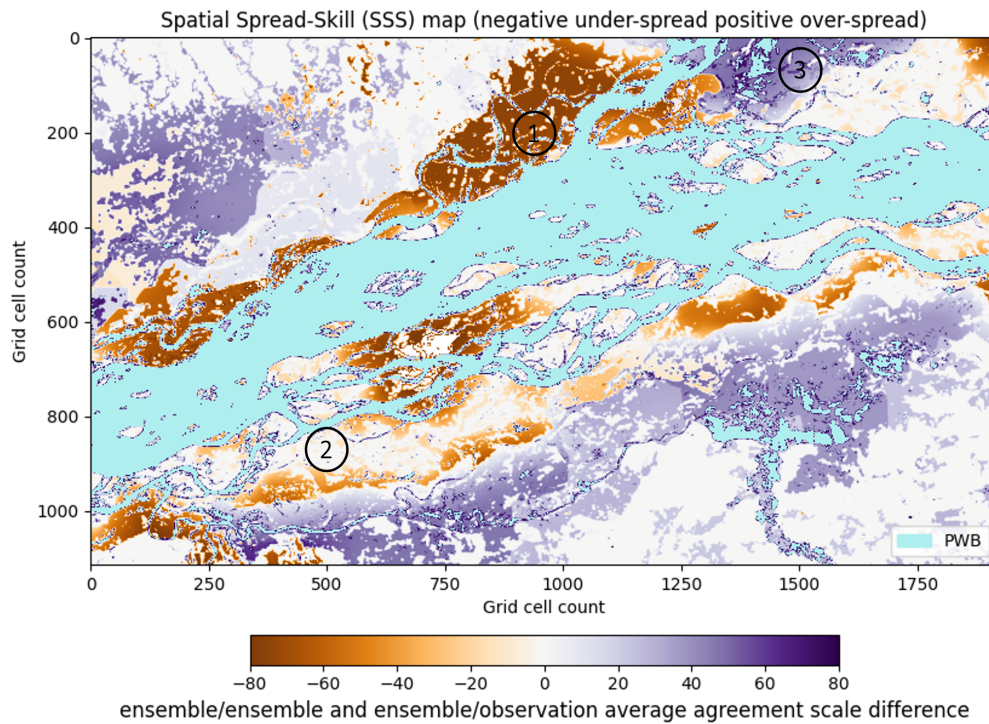
Figure 9. Brahmaputra River, Assam region, August 2017. The Spatial Spread-Skill (SSS) map shows the difference between the ensemble/ensemble and the ensemble/observed average agreement scales at each grid cell. Negative values (orange) indicate where the ensemble is under-spread and positive values (purple) indicate where the ensemble is over-spread. White areas areas indicate where the average agreement scales match and indicate good spatial spread-skill. Areas labelled (1, 2 and 3) are discussed in Section 4.3. For georeferencing see Figure 5. Note PWB means permanent water bodies.

5 Conclusions

Differences between ensemble members in ensemble forecast flood map systems are mostly driven by initial condition perturbations at the top of the hydro-meteorological forecast chain within the NWP system. Presently, there is limited understanding or evaluation of how these meteorological uncertainties link to mapped flooding predictability, which involves additional sources of uncertainty. An evaluation of the spatial predictability and the spread-skill relationship of the ensemble flood map forecast provides an improved understanding of the performance of the forecast system. Uncertainties in other parts of the forecast chain are not truly represented by the ensemble flood maps and evaluating the spatial spread-skill of the flood maps is important for understanding the likelihood of flooding that the ensemble flood maps capture. In this paper, we present a new scale-selective approach to assess the spatial predictability and spread-skill of an ensemble flood map forecast by comparing against a satellite SAR-derived observation of flooding extent. By calculating a skilful scale at each grid cell for every unique ensemble member pair we can determine the ensemble *spatial spread*, and between every ensemble member and the SAR-derived flood map we can determine the ensemble *spatial skill*. The hexbin scatter plot summarises the spread-skill relationship so that a trend across the whole domain can be assessed. The difference between these skilful scales can be mapped onto our new Spatial Spread Skill (SSS) map which shows for each specific location in the domain whether the ensemble is over-, under- or well-spread. The methods are applied to an example flooding event of the Brahmaputra River in the Assam region of India in August 2017.

In operational practice there are multiple options of ensemble flood map presentation type such as presenting the ensemble median or other exceedance probability for delivery to end-users and decision makers. An important aspect of developing an inundation flood forecasting system is to determine the most useful way to present a spatial ensemble forecast. Using a scale-selective approach we have evaluated the performance of individual ensemble members, a combined total ensemble and the spatial ensemble median compared to a SAR-derived observation of flooding extent. Other options could be to exclude ensemble member outliers, to spatially cluster similar ensemble members into groups of flooding extent or to present a most likely, best and worst case ensemble flood map. Whichever presentation method is chosen, this should be fully explored using the spatial spread-skill methods described here to evaluate the ensemble performance of historical flooding events. We found for this example flooding event that one ensemble member significantly outperformed the combined and median flood maps and that potentially in some flood forecasting scenarios this member would have been excluded as an outlier. The categorical scale maps show the ensemble spatial median could miss vital flooding information and that all members should be considered as potential future flooding scenarios.

Through mapping the spatial-spread skill relationship, which varies with location, links can be made between the spatial variations in spread-skill and the physical characteristics of the flooding event. We found that one ensemble member outperformed all others in a region close to a confluence zone and nearby observed heavy rainfall. The region correlates to an area of under-spread ensemble members indicating that not enough members were predicting flooding here. Future studies could investigate the physical processes further using the methods presented here. The ensemble flood map spatial spread-skill is

investigated in the context of a particular physical process (such as rainfall intensity/location or an improved aspect of the hydrological model such as antecedent soil moisture) and how these uncertainties translate to the probabilistic flood map forecast.

460 An understanding of the spatial predictability is particularly important for un-gauged catchments where the calibration of both forecast streamflow and return period thresholds (used to select the simulation library flood map) are rarely practiced routinely. Ideally, in operational practice, these spatial verification approaches including the categorical scale and SSS maps could be calculated and stored routinely as flooding events coincide with SAR-derived or other remotely observed flood maps to build up a verification catalogue/database. This database could then be used to investigate the spatial spread-skill model performance

465 under different scenarios such as forecast lead time, month or season, or flood type. More locally, the impact of an improved DTM or the inclusion of a Digital Surface Model (DSM) or other surface features in the hydraulic model such as embankments could be considered. Over time, such a database would improve our understanding of the spatial predictability of an ensemble flood map system and how well the uncertainties present are represented by the ensemble forecast.

470 *Code and data availability.* The functions used to evaluate the ensemble forecast flood maps using a scale-selective approach along with the SAR-derived flood maps are available on the following Zenodo page: https://doi.org/10.5281/zenodo.6603101 (Hooker et al., 2022b). The forecast flood maps from the JBA Flood Foresight system are commercial data used under license for this study.

Author contributions. JB and KS provided the forecast data. HH wrote the algorithms and ran the experiments, with input from SD, DM, JB and KS. HH prepared the manuscript with contributions from all the co-authors.

475 *Competing interests.* The authors declare that no competing interests are present.

Acknowledgements. This work was supported in part by the Natural Environment Research Council as part of a SCENARIO funded PhD project with a CASE award from the JBA Trust (NE/S007261/1). SD and DM were funded in part by the UK EPSRC DARE project (EP/P002331/1). SD also received funding from NERC National Centre for Earth Observation.

References

480 Alfieri, L., Burek, P., Dutra, E., Krzeminski, B., Muraro, D., Thielen, J., and Pappenberger, F.: GloFAS-global ensemble streamflow forecasting and flood early warning, Hydrology and Earth System Sciences, 17, 1161–1175, https://doi.org/10.5194/hess-17-1161-2013, 2013.

Alfonso, L., Mukolwe, M. M., and Di Baldassarre, G.: Probabilistic Flood Maps to support decision-making: Mapping the Value of Information, Water Resources Research, 52, 1026–1043, https://doi.org/10.1002/2015WR017378, 2016.

Anderson, S. R., Csima, G., Moore, R. J., Mittermaier, M., and Cole, S. J.: Towards operational joint river flow and precipi-
485 tation ensemble verification: considerations and strategies given limited ensemble records, Journal of Hydrology, 577, 123 966, https://doi.org/10.1016/j.jhydrol.2019.123966, 2019.

Arnal, L., Anspoks, L., Manson, S., Neumann, J., Norton, T., Stephens, E., Wolfenden, L., and Cloke, H. L.: "Are We talking just a bit of water out of bank? or is it Armageddon?" Front line perspectives on transitioning to probabilistic fluvial flood forecasts in England, Geoscience Communication, 3, 203–232, https://doi.org/10.5194/gc-3-203-2020, 2020.

490 ASDMA: Assam State Disaster Management Authority Flood Alert, http://sdmassam.nic.in/download/alerts/10.08.2017.jpg, last access 10th November 2021, 2017.

Ben Bouallègue, Z. and Theis, S. E.: Spatial techniques applied to precipitation ensemble forecasts: From verification results to probabilistic products, Meteorological Applications, 21, 922–929, https://doi.org/10.1002/met.1435, 2014.

Beven, K.: Facets of uncertainty: Epistemic uncertainty, non-stationarity, likelihood, hypothesis testing, and communication, Hydrological
495 Sciences Journal, 61, 1652–1665, https://doi.org/10.1080/02626667.2015.1031761, 2016.

Boelee, L., Lumbroso, D. M., Samuels, P. G., and Cloke, H. L.: Estimation of uncertainty in flood forecasts—A comparison of methods, Journal of Flood Risk Management, https://doi.org/10.1111/jfr3.12516, 2019.

Bradbrook, K.: JFLOW: A multiscale two-dimensional dynamic flood model, Water and Environment Journal, https://doi.org/10.1111/j.1747-6593.2005.00011.x, 2006.

500 Buizza, R.: Potential forecast skill of ensemble prediction and spread and skill distributions of the ECMWF ensemble prediction system, Monthly Weather Review, 125, 99–119, https://doi.org/10.1175/1520-0493(1997)125<0099:PFSOEP>2.0.CO;2, 1997.

Central Water Commission: Flood Forecast Dashboard, https://cwc.gov.in/ffm_dashboard, last access 23rd January 2023, 2023.

Chen, X., Yuan, H., and Xue, M.: Spatial spread-skill relationship in terms of agreement scales for precipitation forecasts in a convection-allowing ensemble, Quarterly Journal of the Royal Meteorological Society, 144, 85–98, https://doi.org/10.1002/qj.3186, 2018.

505 Chini, M., Hostache, R., Giustarini, L., and Matgen, P.: A hierarchical split-based approach for parametric thresholding of SAR images: Flood inundation as a test case, IEEE Transactions on Geoscience and Remote Sensing, 55, 6975–6988, https://doi.org/10.1109/TGRS.2017.2737664, 2017.

Cloke, H. L. and Pappenberger, F.: Ensemble flood forecasting: A review, Journal of Hydrology, 375, 613–626, https://doi.org/10.1016/j.jhydrol.2009.06.005, 2009.

510 Cooper, E. S., Dance, S. L., Garcia-Pintado, J., Nichols, N. K., and Smith, P. J.: Observation impact, domain length and parameter estimation in data assimilation for flood forecasting, Environmental Modelling Software, 104, 199–214, https://doi.org/10.1016/J.ENVSOFT.2018.03.013, 2018.

Cooper, E. S., Dance, S. L., García-Pintado, J., Nichols, N. K., and Smith, P. J.: Observation operators for assimilation of satellite observations in fluvial inundation forecasting, Hydrology and Earth System Sciences, 23, 2541–2559, https://doi.org/10.5194/hess-23-2541-2019,
515 2019.

Copernicus Programme: Copernicus Emergency Management Service, https://emergency.copernicus.eu/, last access 14th September 2021, 2021.

Dasgupta, A., Grimaldi, S., Ramsankaran, R., Pauwels, V. R. N., Walker, J. P., Chini, M., Hostache, R., and Matgen, P.: Flood Mapping Using Synthetic Aperture Radar Sensors From Local to Global Scales, pp. 55–77, https://doi.org/10.1002/9781119217886.ch4, 2018a.

Dasgupta, A., Grimaldi, S., Ramsankaran, R. A., Pauwels, V. R., and Walker, J. P.: Towards operational SAR-based flood mapping using neuro-fuzzy texture-based approaches, Remote Sensing of Environment, 215, 313–329, https://doi.org/10.1016/j.rse.2018.06.019, 2018b.

Dasgupta, A., Hostache, R., Ramasankaran, R., Schumann, G. J., Grimaldi, S., Pauwels, V. R. N., and Walker, J. P.: On the impacts of observation location, timing and frequency on flood extent assimilation performance, Water Resources Research, https://doi.org/10.1029/2020wr028238, 2021a.

Dasgupta, A., Hostache, R., Ramsankaran, R. A., Schumann, G. J., Grimaldi, S., Pauwels, V. R., and Walker, J. P.: A Mutual Information-Based Likelihood Function for Particle Filter Flood Extent Assimilation, Water Resources Research, 57, 1–28, https://doi.org/10.1029/2020WR027859, 2021b.

Dey, S. R., Leoncini, G., Roberts, N. M., Plant, R. S., and Migliorini, S.: A spatial view of ensemble spread in convection permitting ensembles, Monthly Weather Review, https://doi.org/10.1175/MWR-D-14-00172.1, 2014.

Dey, S. R., Roberts, N. M., Plant, R. S., and Migliorini, S.: A new method for the characterization and verification of local spatial predictability for convective-scale ensembles, Quarterly Journal of the Royal Meteorological Society, https://doi.org/10.1002/qj.2792, 2016.

Dhar, O. N. and Nandargi, S.: A study of floods in the Brahmaputra basin in India, International Journal of Climatology, 20, 771–781, https://doi.org/10.1002/1097-0088(20000615)20:7<771::AID-JOC518>3.0.CO;2-Z, 2000.

Dhar, O. N. and Nandargi, S.: Hydrometeorological Aspects of Floods in India, pp. 1–33, Springer Netherlands, Dordrecht, https://doi.org/10.1007/978-94-017-0137-2_1, 2003.

Di Mauro, C., Hostache, R., Matgen, P., Pelich, R., Chini, M., Van Leeuwen, P. J., Nichols, N. K., and Blöschl, G.: Assimilation of probabilistic flood maps from SAR data into a coupled hydrologic-hydraulic forecasting model: A proof of concept, Hydrology and Earth System Sciences, 25, 4081–4097, https://doi.org/10.5194/hess-25-4081-2021, 2021.

Emerton, R. E., Stephens, E. M., Pappenberger, F., Pagano, T. C., Weerts, A. H., Wood, A. W., Salamon, P., Brown, J. D., Hjerdt, N., Donnelly, C., Baugh, C. A., and Cloke, H. L.: Continental and global scale flood forecasting systems, Wiley Interdisciplinary Reviews: Water, 3, 391–418, https://doi.org/10.1002/wat2.1137, 2016.

ESA: ICEYE commercial satellites join the EU Copernicus programme, https://www.esa.int/Applications/Observing_the_Earth/Copernicus/ICEYE_commercial_satellites_join_the_EU_Copernicus_programme, last access 28th October 2021, 2021.

EU Science Hub: The Joint Research Centre launches a revolutionary tool for monitoring ongoing floods worldwide as part of the Copernicus Emergency Management Service, https://ec.europa.eu/jrc/en/news/jrc-launches-revolutionary-tool-for-monitoring-floods-worldwide-part-copernicus-emergency-management-service, last access 28th October 2021, 2021.

Floodlist: India – Third Wave of Flooding Hits Assam, 2 Million Affected, http://floodlist.com/asia/india-assam-floods-august-2017, last access 10th November 2021, 2017.

Galmiche, N., Hauser, H., Spengler, T., Spensberger, C., Brun, M., and Blaser, N.: Revealing Multimodality in Ensemble Weather Prediction, 2021.

García-Pintado, J., Mason, D. C., Dance, S. L., Cloke, H. L., Neal, J. C., Freer, J., and Bates, P. D.: Satellite-supported flood forecasting in river networks: A real case study, Journal of Hydrology, 523, 706–724, https://doi.org/10.1016/J.JHYDROL.2015.01.084, 2015.

GFM: GloFAS global flood monitoring (GFM), https://www.globalfloods.eu/technical-information/glofas-gfm/, last access 28th October 2021, 2021.

GloFAS: GloFAS Methods, https://www.globalfloods.eu/general-information/glofas-methods/, last access 15th November 2021, 2021.

Hooker, H., Dance, S. L., Mason, D. C., Bevington, J., and Shelton, K.: Spatial scale evaluation of forecast flood inundation maps, Journal of Hydrology, p. 128170, https://doi.org/https://doi.org/10.1016/j.jhydrol.2022.128170, 2022a.

Hooker, H., Dance, S. L., Mason, D. C., Bevington, J., and Shelton, K.: Ensemble flood map spatial verification [Data set], https://doi.org/10.5281/zenodo.6603101, 2022b.

Hopson, T. M.: Assessing the ensemble spread-error relationship, Monthly Weather Review, 142, 1125–1142, https://doi.org/10.1175/MWR-D-12-00111.1, 2014.

Horritt, M. S., Mason, D. C., and Luckman, A. J.: Flood boundary delineation from synthetic aperture radar imagery using a statistical active contour model, International Journal of Remote Sensing, 22, 2489–2507, https://doi.org/10.1080/01431160116902, 2001.

Hossain, S., Cloke, H. L., Ficchì, A., Turner, A. G., and Stephens, E. M.: Hydrometeorological drivers of flood characteristics in the Brahmaputra river basin in Bangladesh, Hydrology and Earth System Sciences Discussions, 2021, 1–28, https://doi.org/10.5194/hess-2021-97, 2021.

Hostache, R., Chini, M., Giustarini, L., Neal, J., Kavetski, D., Wood, M., Corato, G., Pelich, R. M., and Matgen, P.: Near-Real-Time Assimilation of SAR-Derived Flood Maps for Improving Flood Forecasts, Water Resources Research, 54, 5516–5535, https://doi.org/10.1029/2017WR022205, 2018.

Hostache, R.: A first evaluation of the future CEMS systematic global flood monitoring product, https://events.ecmwf.int/event/222/contributions/2274/attachments/1280/2347/Hydrological-WS-Hostache.pdf, last access 4th August 2021, 2021.

Konapala, G., Kumar, S. V., and Khalique Ahmad, S.: Exploring Sentinel-1 and Sentinel-2 diversity for flood inundation mapping using deep learning, ISPRS Journal of Photogrammetry and Remote Sensing, 180, 163–173, https://doi.org/10.1016/J.ISPRSJPRS.2021.08.016, 2021.

Lehner, B. and Grill, G.: Global river hydrography and network routing: baseline data and new approaches to study the world's large river systems, Hydrological Processes, 27, 2171–2186, https://doi.org/https://doi.org/10.1002/hyp.9740, 2013.

Leutbecher, M. and Palmer, T. N.: Ensemble forecasting, Journal of Computational Physics, 227, 3515–3539, https://doi.org/10.1016/J.JCP.2007.02.014, 2008.

Lorenz, E. N.: The predictability of a flow which possesses many scales of motion, Tellus, 21, 289–307, https://doi.org/10.3402/tellusa.v21i3.10086, 1969.

Mason, D. C., Schumann, G. J., Neal, J. C., Garcia-Pintado, J., and Bates, P. D.: Automatic near real-time selection of flood water levels from high resolution Synthetic Aperture Radar images for assimilation into hydraulic models: A case study, Remote Sensing of Environment, https://doi.org/10.1016/j.rse.2012.06.017, 2012.

Mason, D. C., Dance, S. L., Vetra-Carvalho, S., and Cloke, H. L.: Robust algorithm for detecting floodwater in urban areas using synthetic aperture radar images, Journal of Applied Remote Sensing, 12, 1, https://doi.org/10.1117/1.jrs.12.045011, 2018.

Mason, D. C., Dance, S. L., and Cloke, H. L.: Floodwater detection in urban areas using Sentinel-1 and WorldDEM data, Journal of Applied Remote Sensing, 15, 1–22, https://doi.org/10.1117/1.jrs.15.032003, 2021a.

Mason, D. C., Bevington, J., Dance, S. L., Revilla-Romero, B., Smith, R., Vetra-Carvalho, S., and Cloke, H. L.: Improving urban flood mapping by merging synthetic aperture radar-derived flood footprints with flood hazard maps, Water (Switzerland), 13, https://doi.org/10.3390/w13111577, 2021b.

Matthews, G., Barnard, C., Cloke, H., Dance, S. L., Jurlina, T., Mazzetti, C., and Prudhomme, C.: Evaluating the impact of post-processing medium-range ensemble streamflow forecasts from the European Flood Awareness System, Hydrology and Earth System Sciences, 26, 2939–2968, https://doi.org/10.5194/hess-26-2939-2022, 2022.

595   NEXTmap: NEXTMap World30 DSM, https://www.intermap.com/nextmap, last access 24th January 2023, 2016.

Palash, W., Akanda, A. S., and Islam, S.: The record 2017 flood in South Asia: State of prediction and performance of a data-driven requisitely simple forecast model, Journal of Hydrology, 589, https://doi.org/10.1016/j.jhydrol.2020.125190, 2020.

Pappenberger, F., Beven, K. J., Hunter, N. M., Bates, P. D., Gouweleeuw, B. T., Thielen, J., and de Roo, A. P.: Cascading model uncertainty from medium range weather forecasts (10 days) through a rainfall-runoff model to flood inundation predictions within the European Flood

600   Forecasting System (EFFS), Hydrology and Earth System Sciences, 9, 381–393, https://doi.org/10.5194/hess-9-381-2005, 2005.

Pekel, J. F., Cottam, A., Gorelick, N., and Belward, A. S.: High-resolution mapping of global surface water and its long-term changes, Nature, 540, 418–422, https://doi.org/10.1038/nature20584, 2016.

Renner, M., Werner, M. G., Rademacher, S., and Sprokkereef, E.: Verification of ensemble flow forecasts for the River Rhine, Journal of Hydrology, 376, 463–475, https://doi.org/10.1016/j.jhydrol.2009.07.059, 2009.

605   Roberts, N. M. and Lean, H. W.: Scale-selective verification of rainfall accumulations from high-resolution forecasts of convective events, Monthly Weather Review, https://doi.org/10.1175/2007MWR2123.1, 2008.

Savage, J. T. S., Bates, P., Freer, J., Neal, J., and Aronica, G.: When does spatial resolution become spurious in probabilistic flood inundation predictions?, Hydrological Processes, 30, 2014–2032, https://doi.org/10.1002/hyp.10749, 2016.

Speight, L. and Krupska, K.: Understanding the impact of climate change on inland flood risk in the UK, Weather, 76, 330–331,

610   https://doi.org/10.1002/wea.4079, 2021.

Tavus, B., Kocaman, S., Nefeslioglu, H. A., and Gokceoglu, C.: A fusion approach for flood mapping using sentinel-1 and sentinel-2 datasets, International Archives of the Photogrammetry, Remote Sensing and Spatial Information Sciences - ISPRS Archives, 43, 641–648, https://doi.org/10.5194/isprs-archives-XLIII-B3-2020-641-2020, 2020.

WMO: South Asian Climate Outlook Forum held in Bhutan, https://public.wmo.int/en/media/news/

615   normal-rainfall-likely-much-of-south-asia-2017-southwest-monsoon, last access 23rd January 2023, 2017.

Wu, W., Emerton, R., Duan, Q., Wood, A. W., Wetterhall, F., and Robertson, D. E.: Ensemble flood forecasting: Current status and future opportunities, WIREs Water, 7, 1–32, https://doi.org/10.1002/wat2.1432, 2020.

Zappa, M., Jaun, S., Germann, U., Walser, A., and Fundel, F.: Superposition of three sources of uncertainties in operational flood forecasting chains, Atmospheric Research, 100, 246–262, https://doi.org/10.1016/J.ATMOSRES.2010.12.005, 2011.